

Phase transition of iron sulphide minerals under hydrothermal conditions and magnetic investigations

Ssu Han Li¹ · Yen-Hua Chen¹ · Jey-Jau Lee² · Hwo-Shuenn Sheu²

Received: 6 December 2016 / Accepted: 15 May 2017 / Published online: 24 May 2017
© Springer-Verlag Berlin Heidelberg 2017

Abstract Iron sulphide minerals have been used in industrial applications for many years, and more recently there has been increasing interest in the use of iron sulphide nanomaterials because of their useful properties and low cost. Previous studies have mainly focused on the synthesis of iron sulphides, but their phase transition and micro-magnetic properties are still unclear. In this study, iron sulphide minerals were synthesized via a hydrothermal method, and their phase transition mechanisms and magnetic properties were investigated. Ex situ and in situ X-ray diffraction results of the iron–sulphur system under hydrothermal conditions suggested that the transformation sequence followed the order of mackinawite (FeS) → greigite (Fe₃S₄) → smythite (Fe₉S₁₁) → pyrrhotite (Fe₉S₁₀). Pure greigite and pyrrhotite were obtained during the synthesis processes, after 1 h at 120 and 160 °C, respectively. Greigite showed a granular morphology with particle diameters around 30 nm, and pyrrhotite comprised stacked hexagonal sheets with thousands of nanometers in width. Pyrrhotite showed anti-ferromagnetic behaviour; however, it did not saturate up to magnetic field of 7 T. Greigite was ferrimagnetic, with a high saturation magnetization of 62.7 Am² kg⁻¹ and coercive magnetic field of 27.6 mT. Magnetic force microscope measurements of greigite revealed that its magnetic structure belonged to a spin-canted single domain. Overall, this study provides new information on the phase transition mechanism, related reaction formulas, and magnetic

properties of iron sulphides, and it emphasizes the important role played by temperature/time in phase transitions.

Keywords Greigite · Pyrrhotite · Magnetic structure · Transformation sequence

Introduction

Iron sulphide minerals are present in the Earth's crust in various Fe–S phases, and mackinawite (FeS), greigite (Fe₃S₄), smythite (Fe₉S₁₁), pyrrhotite (Fe_{1-x}S), and pyrite (FeS₂) can be commonly found in nature. These minerals tend to be found in anoxic marine and lake sedimentary systems, hydrothermal systems, and near mid-ocean ridges (Morimoto et al. 1975; Chang et al. 2008; Devey 2009).

Mackinawite was first described by Evans et al. (1962, 1964) and Devey (2009) from samples found in the Snohomish County (USA). Mackinawite is metastable and shows an anti-PbO-type crystal structure with layers of iron–sulphur tetrahedra bonding together via Van der Waals interactions (Lennie et al. 1995; Rickard and Luther 2007; Sines et al. 2012). Mackinawite is commonly regarded as the first iron sulphide phase, which is formed from the reaction of Fe²⁺ with S²⁻ solutions (Rickard and Luther 2007; Sines et al. 2012). Several studies on mackinawite syntheses mimic natural processes, e.g. biological precipitations or co-precipitations of Fe²⁺ and S²⁻ at ambient conditions (Frankel and Bazylinski 2003; Jeong et al. 2008; Sines et al. 2012).

Greigite was first discovered in Californian lacustrine sediments by Skinner et al. (1964), Chang et al. (2008) and Devey (2009). Greigite has an inverse spinel structure and is the sulphide analogue of the iron oxide mineral magnetite (Fe₃O₄) (Roberts and Weaver 2005; Chang et al. 2008;

✉ Yen-Hua Chen
yhc513@mail.ncku.edu.tw

¹ Department of Earth Sciences, National Cheng Kung University, Tainan 701, Taiwan

² National Synchrotron Radiation Research Center, Hsinchu 300, Taiwan

Devey 2009); Fe_3S_4 and Fe_3O_4 have the same cubic crystal structures with octahedral and tetrahedral sites (Letard et al. 2005; Devey 2009). The unit cell of greigite includes 56 atoms, of which 24 are iron and 32 are sulphur. Eight Fe^{3+} atoms are in tetrahedral sites and the other Fe atoms (half Fe^{2+} and half Fe^{3+}) in octahedral sites. Correspondingly, sulphur atoms are formed in a closely packed cubic lattice (Devey 2009).

Smythite was first defined as an iron sulphide by Erd et al. from samples present in calcite crystals from Bloomington (USA) (Erd et al. 1957; Taylor 1970). The chemical composition of smythite was determined to be Fe_3S_4 by Erd et al. (1957), and the composition was revised and later reconfirmed to be $(\text{Fe},\text{Ni})_9\text{S}_{11}$ by Taylor and Williams (1972). The crystal structure of smythite has a, NiAs-derivative structure, and rhombohedral stacking of sulphur atoms is evident along the *c* axis. Moreover, smythite is strongly ferromagnetic (Erd et al. 1957). Synthesis of smythite was originally accomplished by Rickard (1968) at 25 °C and 1 atm. In nature, smythite is usually found associated with rhombohedral carbonates (Rickard and Luther 2007).

Pyrrhotite (Fe_{1-x}S , with $x = 0\text{--}0.13$) can be widely found in nature and has a crystal structure with alternating iron and sulphur layers, similar to the NiAs crystal structure. Morimoto et al. (1975) studied pyrrhotite from different geological conditions and their results revealed abundant and widespread occurrences of three different pyrrhotites, namely, 4C (Fe_7S_8), nC (intermediate pyrrhotite, ranging from Fe_9S_{10} to $\text{Fe}_{11}\text{S}_{12}$, and usually with non-integral types of superstructure), and 2C (troilite). The 4C form is ferrimagnetic monoclinic, and the 5C, 11C, and 6C forms are anti-ferromagnetic hexagonal forms (Morimoto et al. 1975; Dekkers 1988). All of the iron atoms in pyrrhotite are present as Fe^{2+} , and sulphur atoms have a chemical state of <2. Pyrrhotite often contains some vacancies, which are dependent on its chemical composition, and the vacancy distribution has been shown to be in relation to its magnetic properties (Dekkers 1988).

There is increasing interest in iron sulphide nanomaterials owing to their low cost and low toxicity, which make them competitive materials for electronic, magnetic, and photoelectric applications (He et al. 2006; Gong et al. 2013; Li et al. 2015). For example, mackinawite has been used in environmental remediation work, where it has been shown to effectively immobilize heavy metals and toxic ions through sorption mechanisms (Watson et al. 1995; Holmes 1999; Mullet et al. 2004; Wolthers et al. 2005; Cs akber enyi-Malasics et al. 2012). Greigite is important for palaeomagnetic and environmental magnetic studies (Krupp 1994; Roberts and Weaver 2005; Chang et al. 2008; Gao et al. 2015) and it has also attracted attention as an anode material for lithium ion batteries (Apostolova et al. 2009; Li

et al. 2015); moreover, it has been investigated and utilized for hyperthermia treatments in biomedicine (Johannsen et al. 2005; Chang et al. 2011; Paoletta et al. 2011; Feng et al. 2013 Vallejo-Fernandez et al. 2013). Pyrrhotite geothermometry has been applied to determine the temperature of ore bodies (Gupta 1965; Nekrasov and Besmen 1979). Finally, iron sulphides have been studied for nuclear waste storage applications in France (Bourdoiseau et al. 2011).

Because of the geological significance and numerous industrial applications of iron sulphide minerals, detailed understanding of their phase transformations and magnetic properties would be valuable. However, the formation pathways of iron sulphides are still not fully understood (Schoonen and Barnes 1991; Krupp 1994; Cahill et al. 2000). Previous work has mostly focused on the synthesis of iron sulphide minerals rather than on investigations of their physical properties (Taylor et al. 1979; Schoonen and Barnes 1991; Cahill et al. 2000; Chen et al. 2005; White et al. 2015). Several studies have investigated high-temperature phase transitions beyond 200 °C, but few have looked at transitions below 200 °C, and the mechanism of phase transition and related reaction formulas has not been examined (Lennie et al. 1997; Beal et al. 2012; Yuan et al. 2012; Gao et al. 2015). In this study, iron sulphide minerals were synthesized by hydrothermal methods under anoxic conditions. Comparisons of ex situ and in situ experimental results allowed phase transition mechanisms to be identified, and magnetic properties at the micro- and macro-scale were also examined.

Experimental

Ex situ experiments

For ex situ experiments, thioacetamide (15 mmol) and $\text{FeSO}_4 \cdot 7\text{H}_2\text{O}$ (10 mmol) were dissolved in 50 mL oxygen-free deionized water in a plastic glove box (Chen et al. 2005), and the solution was transferred to a 300 mL Teflon-lined stainless steel autoclave. The autoclave was sealed and maintained at different temperatures (120, 130, 140, 150, 160 and 170 °C) for 1 h for the different experiments, and then samples were allowed to cool down to room temperature. The precipitates were then filtered and washed with oxygen-free distilled water and pure ethanol several times. Lastly, the samples were freeze-dried for 6 h.

An X-ray powder diffractometer (XRD, Bruker D8 Advanced, $\text{Cu-K}\alpha$) was used to identify the crystal structure of iron sulphides subjected to different experimental treatments. The analysis was carried out at ambient conditions, and the scan range was $2\theta = 15^\circ\text{--}60^\circ$ (a scanning speed of $1^\circ/\text{min}$, step size 0.02°). The morphology of specimens was observed by transmission electron microscopy (TEM, Hitachi H-7500) with a tungsten filament and an accelerating

voltage of 40–120 kV; the selected area electron diffraction (SAED) was also performed to examine the mineral phase. The sample preparation for TEM (SAED) measurements was described as follows. The sample powders were dispersed in 100% deoxygenated ethanol and one drop was deposited onto a standard TEM support film (lacey carbon film on gold 200 mesh) and then dried at room temperature. These processes were all performed inside the glove box. Magnetic measurements were carried out via a superconducting quantum interference device (SQUID, MPMS-XL7, Joint Center for high valued Instruments of Taiwan) and magnetic force microscopy (MFM, Bruker, Innova).

In situ experiments

For in situ analyses, precursor solutions were prepared following the same procedures as for the ex situ experiments described above. Solutions were then put into individual 35-mm-long quartz capillaries with 1.0 mm outer diameters, which were sealed by using two parts filled black epoxy with high-viscosity catalysts. The whole procedure was conducted in a plastic glove box to avoid sample oxidation. The in situ XRD experiment was carried out on the BL17A1 and BL01C2 beamlines at the National Synchrotron Radiation Research Center (NSRRC) TLS light source in Taiwan. The ring energy of TLS was operated at 1.5 GeV with a typical current of 360 mA in the TOP-UP mode. The wavelengths of the incident X-rays were 1.32 Å (BL17A1) and 1.03 Å (BL01C2) delivered from the superconducting wavelength-shifting magnet and an Si(111) triangular crystal monochromator (TCM). The diffraction patterns were recorded using a Mar345 imaging plate detector approximately 180 mm away from sample positions and with typical exposure duration of 6 min (BL17A1) or 3 min (BL01C2). The pixel size of Mar345 was 100 μm. The two-dimensional diffraction pattern was converted to one-dimensional powder diffraction profile by program GSAS-II and cake-type integration. The diffraction angles were calibrated according to Bragg positions of LaB₆ standards. All the data presented in our figures were transformed to Cu-wavelength data. Samples were heated to the required temperature (120, 130, 140, 150, and 160 °C), and the temperature was maintained for 1 or 2 h. Real-time XRD measurements were performed after the required temperature was reached and at every adjustment interval.

Results

Ex situ results

The XRD patterns of iron sulphides synthesized under hydrothermal conditions at different reaction temperatures for 1 h are shown in Fig. 1. Cubic greigite (Fe₃S₄)

with a lattice parameter of 9.88 Å was obtained at a temperature of 120 °C, which corresponds to the information on the International Center for Diffraction Data (ICDD) card (No. 01-089-1998). When the temperature was increased to 130 °C, smythite (Fe₉S₁₁, ICDD Card No. 00-010-0437) was observed together with minor greigite, and this was maintained up to 140 °C. Greigite gradually disappeared and the peak intensity of smythite decreased; then, pyrrhotite (Fe₉S₁₀, ICDD Card No. 00-029-0724) was obtained at a temperature of 150 °C. Finally, pure pyrrhotite was obtained when the temperature was increased to 160 and 170 °C. The above-mentioned results are summarized in Table 1.

The XRD patterns of iron sulphides synthesized after a temperature of 120 °C and maintained for different time periods are presented in Fig. 2. Greigite appeared at the reaction time of 1 h, while smythite along with minor greigite was observed at 2 h. When the heating time was increased to 3 h, greigite disappeared (or the peak intensity of greigite decreased) and then pyrrhotite occurred. Pure pyrrhotite was obtained with a heating time of up

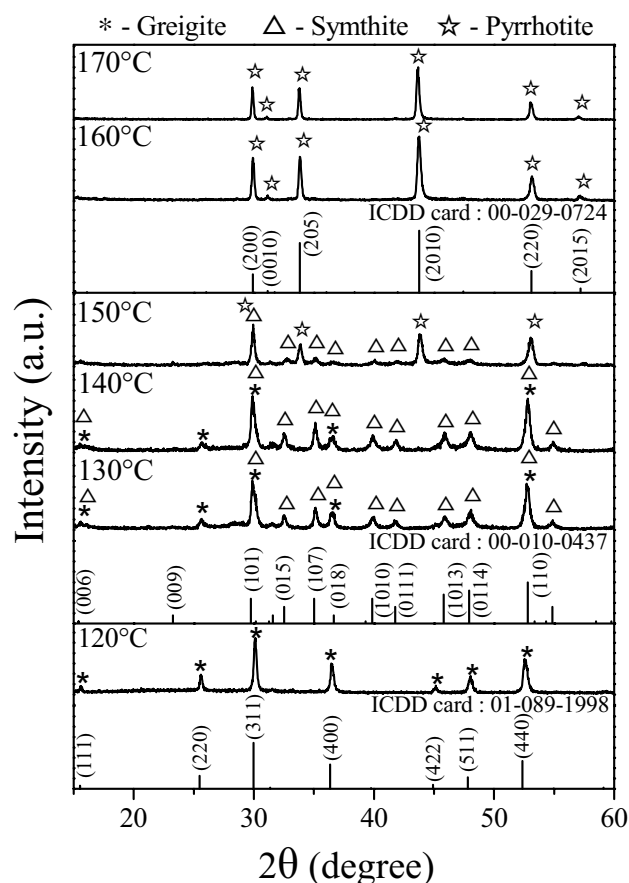


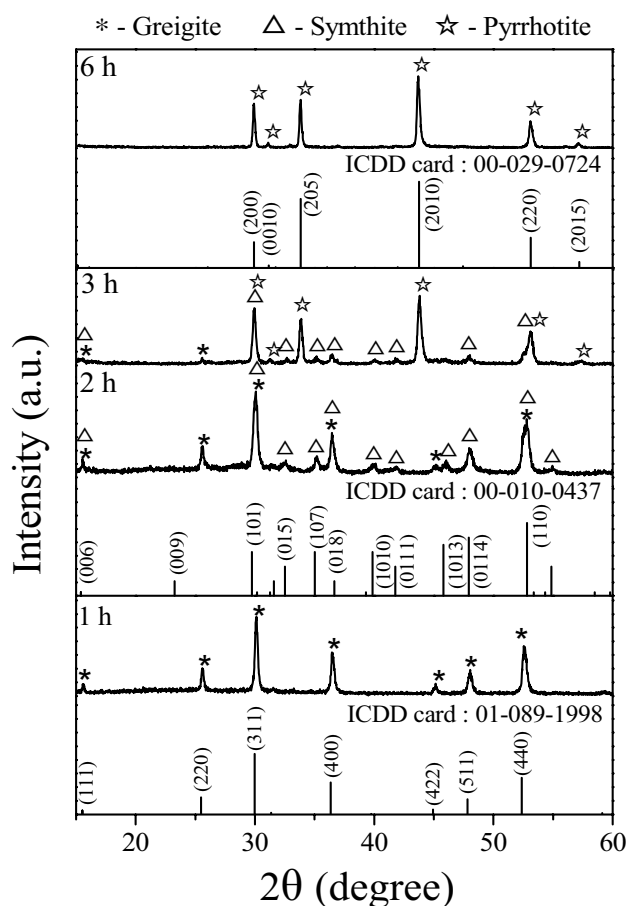
Fig. 1 XRD patterns of iron sulphides synthesized under hydrothermal conditions at different reaction temperatures for 1 h

Table 1 Results of mineral phases for iron sulphides synthesized at different reaction temperatures for the duration time of 1 h

Reaction temperature (°C)	Phase
120	Greigite (Fe ₃ S ₄)
130	Greigite ^b (Fe ₃ S ₄), smythite ^a (Fe ₉ S ₁₁)
140	Greigite ^b (Fe ₃ S ₄), smythite ^a (Fe ₉ S ₁₁)
150	Smythite ^b (Fe ₉ S ₁₁), pyrrhotite ^a (Fe ₉ S ₁₀)
160	Pyrrhotite (Fe ₉ S ₁₀)
170	Pyrrhotite (Fe ₉ S ₁₀)

^a Dominant phase^b Minor amount in the product**Table 2** Summary of products for iron sulphide minerals at 120 °C for different heating times

Heating time (h)	Products
1	Greigite (Fe ₃ S ₄)
2	Greigite ^b (Fe ₃ S ₄), smythite ^a (Fe ₉ S ₁₁)
3	Greigite ^b (Fe ₃ S ₄), smythite ^b (Fe ₉ S ₁₁), Pyrrhotite ^a (Fe ₉ S ₁₀)
6	Pyrrhotite (Fe ₉ S ₁₀)

^a Dominant phase^b Minor amount in the product**Fig. 2** XRD patterns of iron sulphides under crystal growth at 120 °C for various heating times

to 6 h. These results for different heating times at 120 °C are summarized in Table 2.

In situ results

The in situ synchrotron radiation XRD patterns of samples after 1 h at different reaction temperatures are

presented in Fig. 3. At 120 °C, the peak intensity of mackinawite (ICDD Card No. 00-015-0037) was weak (Fig. 3a) and it clearly increased when the temperature was raised to 130 °C (Fig. 3b). The (220), (311), (400), and (440) peaks of greigite appeared when the temperature was maintained at 140 °C (Fig. 3c), and mackinawite was completely transformed into pure greigite at a temperature of 150 °C (Fig. 3d). Greigite persisted at 160 °C; however, its intensity was very weak because of its low concentration of crystallites, the high absorption of water in the sealed quartz capillary, and movement of the sample owing to the high vapour pressure (Fig. 3e). The in situ results for the different temperatures maintained for 1 h are summarized in Table 3.

The in situ XRD patterns of samples at different temperatures maintained for 2 h are shown in Fig. 4. At 120 °C, complete mackinawite peaks were observed along with the (311) and (440) greigite peaks (Fig. 4a). When the temperature was increased to 130 °C, the peak intensity of mackinawite reduced or disappeared and the peak intensity of greigite increased (Fig. 4b). Pyrrhotite, along with minor greigite, was observed at a temperature of 140 °C (Fig. 4c). The in situ results for the different reaction temperatures maintained for 2 h are also summarized in Table 3.

The morphology of pyrrhotite consisted of stacked hexagonal sheets, with individual sheets that were thousands of nanometers in width (Fig. 5a), and its SAED pattern suggested that the structure belonged to pyrrhotite (Fig. 5b). Figure 5c shows a TEM bright filed image of greigite and the corresponding SAED pattern (Fig. 5d) indicates that greigite is a pure phase. This is because the SAED pattern shows clear and orientated diffraction spots and their d-spacings agreed with those in the XRD pattern, which corresponds to the greigite phase (each mineral phase has its characteristic SAED pattern). This mineral demonstrated an irregular to granular morphology, with a grain size ranging from 30 to 300 nm (Fig. 5e).

Fig. 3 In situ synchrotron XRD patterns of iron sulphide minerals with crystal growth maintained for 1 h with reaction temperatures of **a** 120, **b** 130, **c** 140, **d** 150, and **e** 160 °C

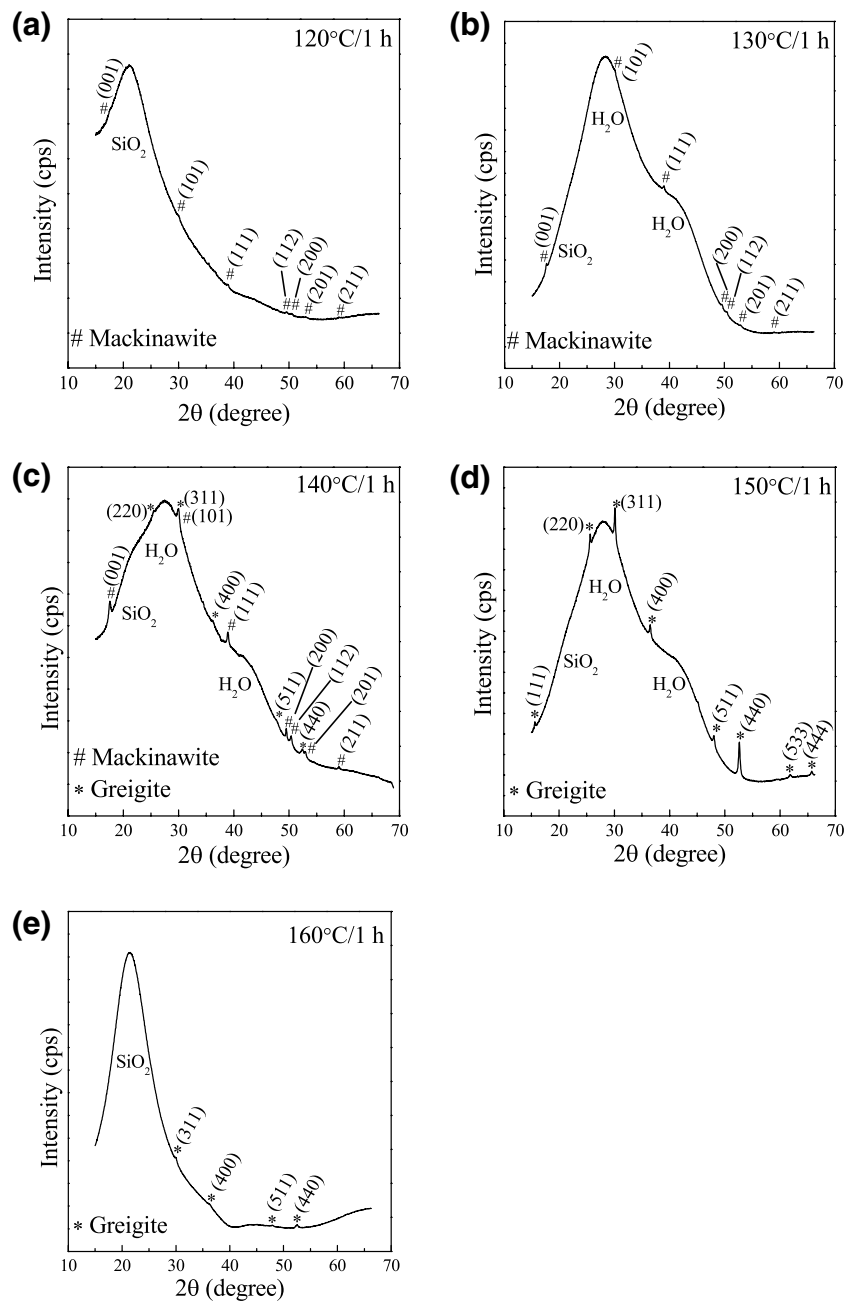


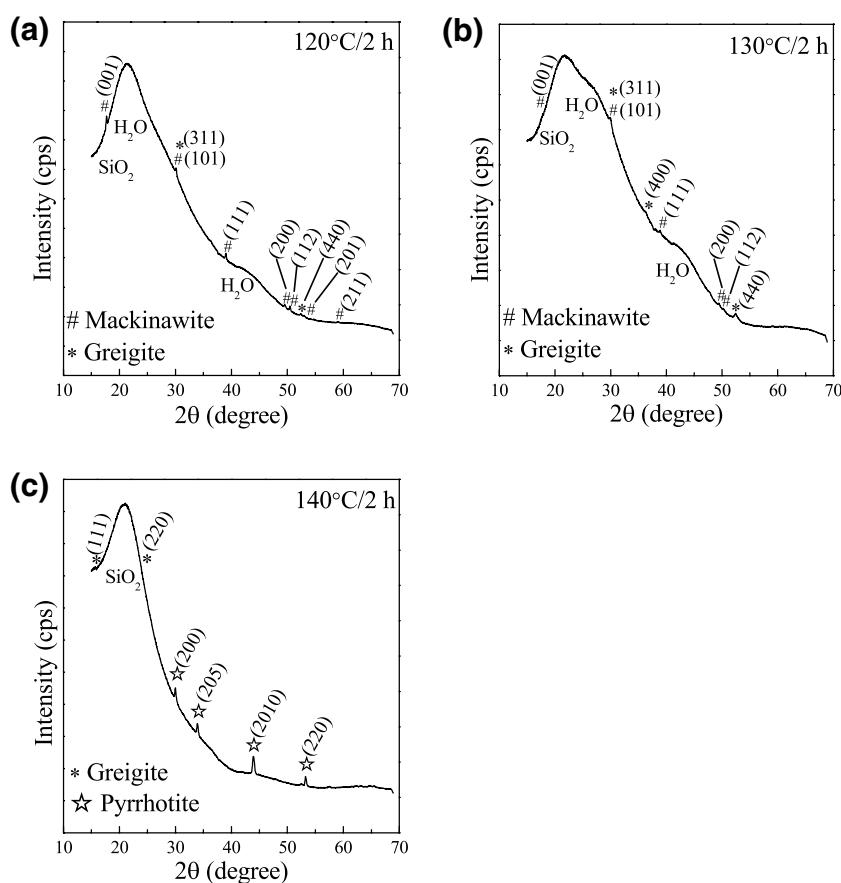
Table 3 List of mineral-phases for in situ synchrotron experiments with different crystal growth conditions

Reaction temperature (°C)	Heating time (h)	Phase
120	1	Mackinawite (FeS)
130	1	Mackinawite (FeS)
140	1	Mackinawite (FeS), greigite (Fe ₃ S ₄)
150	1	Greigite (Fe ₃ S ₄)
160	1	Greigite (Fe ₃ S ₄)
120	2	Mackinawite ^a (FeS), Greigite ^b (Fe ₃ S ₄)
130	2	Mackinawite (FeS), greigite (Fe ₃ S ₄)
140	2	Greigite ^b (Fe ₃ S ₄), pyrrhotite ^a (Fe ₉ S ₁₀)

^a Dominant phase

^b Minor amount in the product

Fig. 4 In situ synchrotron XRD results of iron sulphides with crystal growth maintained for 2 h at different reaction temperatures of **a** 120, **b** 130, and **c** 140 °C



Magnetic properties

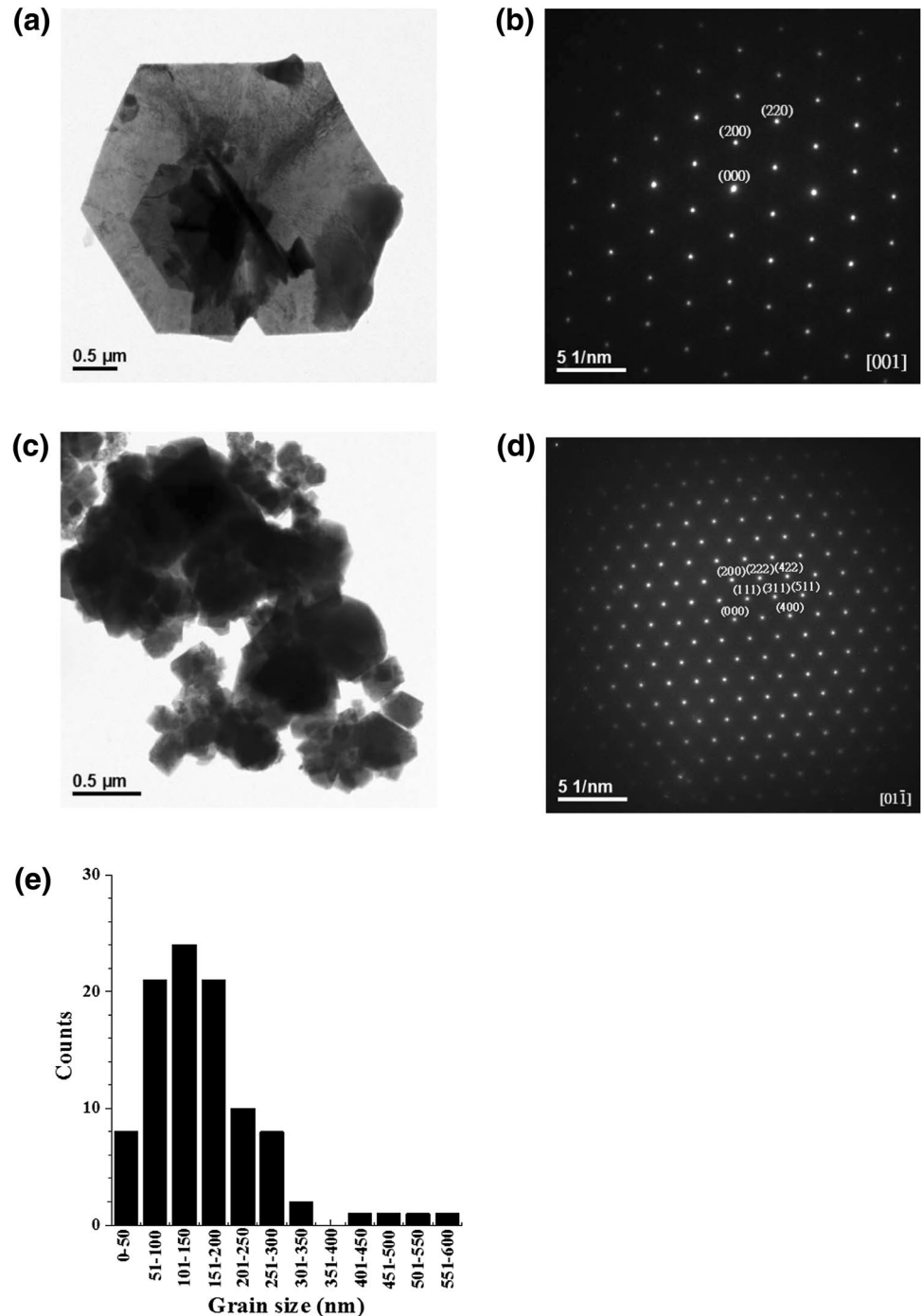
The magnetic properties of pyrrhotite (synthesized at 160 °C for 1 h), as measured by a SQUID at 300 K with a magnetic field up to ± 7 T, are shown in Fig. 6. The pyrrhotite was not yet saturated in this state and its coercive field (B_c) was 84.9 mT. The pyrrhotite belonged to the ferromagnetic type, which is in agreement with earlier studies (Schwarz and Vaughan 1972; Dekkers 1989; Dekkers and Schoonen 1994; Li 1996; Kontny et al. 2000; O'Reilly et al. 2000). The magnetic property of greigite (synthesized at 120 °C for 1 h) was measured at 300 K with ± 1 T (Fig. 7). The hysteresis loop demonstrated ferromagnetic behaviour of greigite with a saturation magnetization (M_s) of $62.7 \text{ Am}^2 \text{ kg}^{-1}$, remanent magnetization (M_{rs}) of $18.1 \text{ Am}^2 \text{ kg}^{-1}$, coercive magnetic field (B_c) of 27.6 mT, and coercive magnetic field remanence (B_{cr}) of 52.5 mT. The M_s , M_{rs} , and B_c were determined from the hysteresis loops, following a paramagnetic slope correction; the B_{cr} was determined from the back-field remanence curves. The M_{rs}/M_s and B_{cr}/B_c ratios were 0.29 and 1.90, respectively. The Day plot is a way of classifying the domain states and grain sizes of magnetic minerals (Day et al. 1977; Parry 1982; Dunlop 2002; Rowan et al. 2009; Fu et al. 2015). Based on the Day plot (Fig. 8), the

greigite synthesized in this study was classified as a single domain (SD) to a pseudo single domain (PSD).

Figure 9a–c shows the MFM topography, phase image, and the magnetic signal of greigite particles, respectively. These showed irregular to granular morphology with a particle size of around 100 nm (Fig. 9a), which corresponds with the TEM image. In the phase image (Fig. 9b), individual nanoparticles presented a white area or a black region or a black and a bright area. In their corresponding magnetic signals (Fig. 9c), the nanoparticles exhibited a positive or a negative signal, or a negative and positive MFM signals, which are characteristic of a single domain (SD) or a pseudo single domain (PSD). However, the magnetic critical size of SD for greigite was around 50–115 or 23–204 or 12–198 nm, which was investigated by Muxworthy and Williams (2009), Roberts et al. (2011), and Muxworthy et al. (2013). Therefore, the magnetic structure of greigite in this study was deemed to be a single domain to a pseudo single domain. In Fig. 9d, a possible magnetic structure for greigite is presented and the data indicated that greigite nanoparticles were magnetic carriers.

Table 4 gives an overview of the main magnetic properties of greigite from the literatures (Uda 1965; Spender et al. 1972; Hoffmann 1992; Dekkers and Schoonen 1996; Chen et al. 2005; Chang et al. 2008; Zhang and Chen

Fig. 5 **a** The low-magnification TEM image of pyrrhotite synthesized at 160 °C for 1 h, **b** SAED pattern corresponding to the [001] of pyrrhotite, **c** TEM image of greigite prepared at 120 °C for 1 h, **d** SAED pattern corresponding to the [01 $\bar{1}$] of greigite and **e** histogram of the grain size distribution for greigite sample as determined from ~100 grain counts from TEM observations



2009), which are compared with the results of this study. Previous studies mostly defined domain states as PSD and SD, and M_s ranges from 3 to 59 Am² kg⁻¹ were observed. The greigite synthesized in this study had a high saturation magnetization (62.7 Am² kg⁻¹), and therefore it may be useful for potential applications in the cancer hyperthermia work (greigite could be a fine candidate for application in cancer hyperthermia because of its high self-heating capacity and low toxicity characteristics. The heating

mechanisms of magnetic nanoparticles for hyperthermia applications are feasible and associated with susceptibility loss and hysteresis loss. A magnetic hyperthermia application with magnetic nanoparticles has been discovered that can reduce tumour size in humans. Therefore, greigite in this study, with a high saturation magnetization, may be suitable for such application in this field) (Johannsen et al. 2005; Chang et al. 2011; Paoletta et al. 2011; Feng et al. 2013; Vallejo-Fernandez et al. 2013).

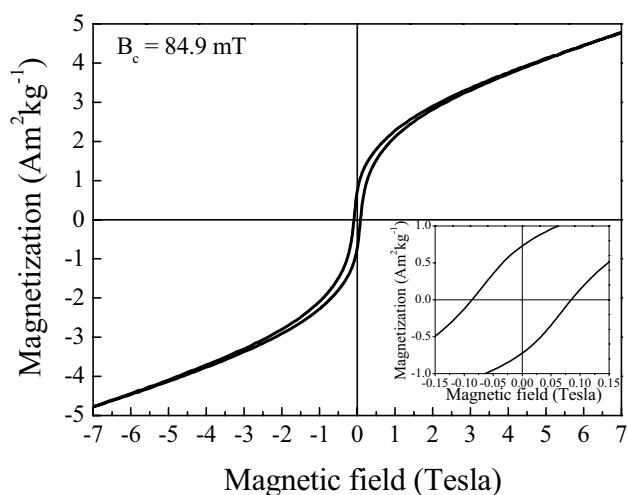


Fig. 6 Magnetic hysteresis curve of the pyrrhotite sample measured at room temperature with a magnetic field up to ± 1 T

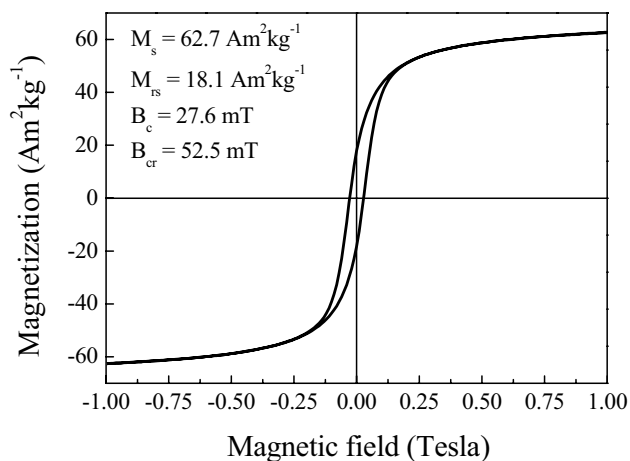


Fig. 7 Magnetic hysteresis curve of the greigite specimen measured at 300 K with a magnetic field up to ± 7 T

Discussion

Mechanism of mackinawite formation

The starting materials used in this study were $\text{FeSO}_4 \cdot 7\text{H}_2\text{O}$ and thioacetamide ($\text{C}_2\text{H}_5\text{NS}$). In an acid solution, hydrolysis of thioacetamide yielded acetamide and hydrogen sulphide at 90 °C (Butler et al. 1958; Bourdoiseau et al. 2011), and then hydrogen sulphide dissociated into S^{2-} . $\text{FeSO}_4 \cdot 7\text{H}_2\text{O}$ acted as the source of Fe^{2+} , thioacetamide generated the S^{2-} source, and then Fe^{2+} reacted with S^{2-} to produce FeS (Sines et al. 2012). The possible reactions were:

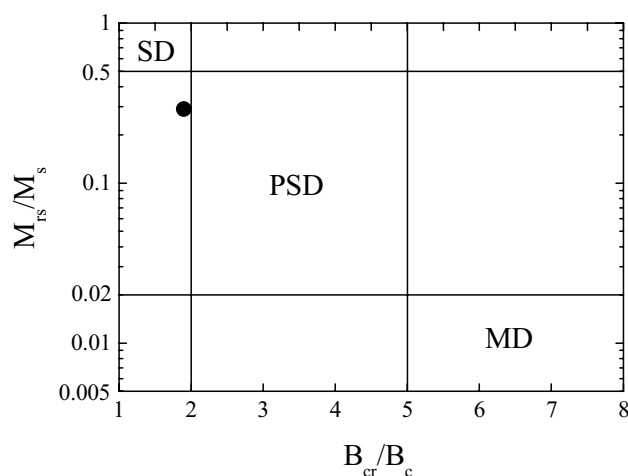
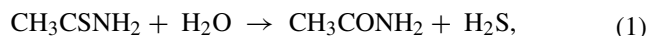
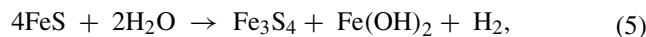


Fig. 8 Day plot (M_{ts}/M_s vs. H_{cr}/H_c) for the greigite sample

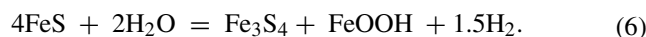


Mackinawite–greigite transition

During the transformation from mackinawite to greigite, Fe^{III} -containing mackinawite constitutes the intermediate between mackinawite $\text{Fe}^{\text{II}}\text{S}$ and greigite $\text{Fe}^{\text{II}}\text{Fe}_2^{\text{III}}\text{S}_4$. Therefore, greigite formation first occurs through oxidation of Fe^{2+} to Fe^{3+} in the mackinawite lattice. However, our experiments were carried out under anoxic solution conditions, which suggest that the reaction may be autocatalytic and anoxic H_2O is the oxidant (Rickard and Luther 2007; White et al. 2015):



or



In this study, no $\text{Fe}(\text{OH})_2$ or FeOOH was found in the XRD pattern [no orange-brown or green precipitates (FeOOH or $\text{Fe}(\text{OH})_2$) appeared during the whole experimental procedure]. Moreover, FeOOH and $\text{Fe}(\text{OH})_2$ would have been stable at $\text{pH} = 7\text{--}9.3$ and above $\text{pH} 11$, respectively (Harrison 2008; Sharma 2012). Therefore, H_2O is not the oxidant in the solution. We speculate that the oxidant may be H_2S (Bourdoiseau et al. 2011), which was produced from CH_3CSNH_2 . The possible reaction was as follows:

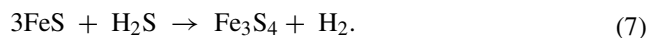


Fig. 9 MFM results of **a** topography, **b** phase image, **c** magnetic signals of greigite particles of *A*, *B*, and *C*, and **d** the corresponding magnetic stray fields of *A*, *B*, and *C* greigite particles (*arrow* is the magnetic direction of the N pole)

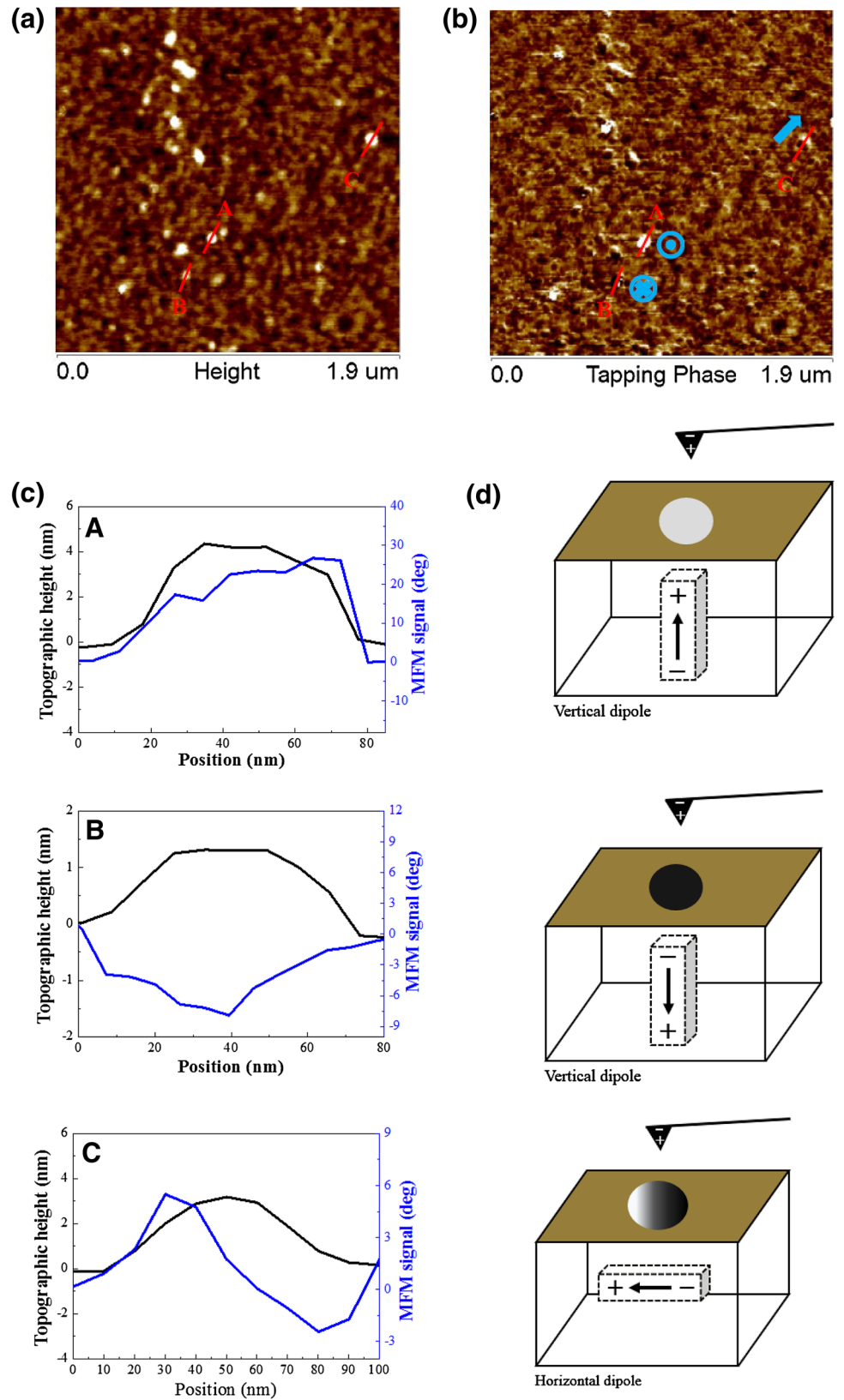


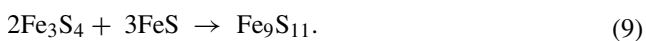
Table 4 Grain size and magnetic properties of greigite synthesized in this study compared to the literature data

Greigite	Grain size (nm)	Domain	B_c	M_s (Am ² kg ⁻¹)	M_{rs}/M_s	References
Synthetic	<1000–44,000	PSD/MD	~7 to 8 mT	59	~0.12	Chang et al. (2008)
Synthetic	10 wide acicular	SD	–	38.5	–	Chen et al. (2005)
Synthetic	100	SD	–	19.7	–	Chen et al. (2005)
Synthetic	30–50	SP	–	24	–	Uda (1965)
Sediment	<4000–8000	PSD/MD	15–30 mT	20	0.35	Hoffmann (1992)
Synthetic				23.1		Zhang and Chen (2009)
				34.0		
Synthetic	<150–400	SP/SD	–	3–29	–	Dekkers and Schoonen (1996)
Synthetic	9–13	–	0.5–3 mT	~34	0.20–0.30	Spender et al. (1972)
Synthetic	30–300	SD/PSD	27.6 mT	62.7	0.29	This study

Greigite–smythite transition

Smythite is known to be obtained from different reaction pathways. For example, smythite can be formed by oriented replacement of mackinawite or greigite (Krupp 1994); it can also be synthesized by a quenching product from pyrrhotite (Fleet 1982) and at 25 °C via siderite reacting with H₂S (aq) (Rickard 1968). Therefore, smythite can appear via controlling the reaction temperature, pH values, starting raw-materials, and so on.

From the observations in this study, we suggest that smythite may be formed via oriented replacement of greigite. This means that the transformation from greigite to smythite may have involved all of the tetrahedrally coordinated iron atoms moving to octahedral sites and some octahedral iron atoms moving into other octahedral sites. There must have been a translation in the sub-lattice (greigite exists in the slightly more iron-rich environment, Krupp 1994). The possible reaction was as follows:



Greigite–pyrrhotite transition

Skinner et al. (1964) heated greigite in sealed, evacuated silica glass tubes. No change occurred after 165 h at 238 °C, and the first evidence of a breakdown occurred after 148 h at 282 °C when approximately 5% of the greigite had broken down to pyrrhotite plus S vapour. It was assumed that the excess sulphur generated from the breakdown was present as a vapour phase in the free space of the silica glass tube. These results indicate that there is a kinetic problem involved, and runs of longer duration transformed greigite into pyrrhotite as follows: $3\text{Fe}_3\text{S}_4 \rightarrow \text{Fe}_9\text{S}_{10} + 2\text{S}_{(g)}$.

The ex situ XRD pattern (Fig. 1) showed that pure greigite was synthesized after 1 h at 120 °C, and then other

phases appeared at different reaction temperatures. The ex situ results allowed the following reaction sequence to be established: greigite → smythite → pyrrhotite. Moreover, the in situ XRD data were able to detect the transformation from mackinawite into greigite because of the higher energy of the synchrotron radiation compared with the laboratory equipment used in the ex situ analysis. This demonstrated that mackinawite is the first mineral phase in the formation pathway of iron sulphides. Fe₉S₁₁ was not observed in the in situ XRD patterns; this may have been due to the Fe₉S₁₁ being metastable, and thus the process of transformation was too fast for detection.

In this study, similar results were observed in ex situ and in situ experiments, and the same reaction pathway was suggested (Tables 1, 3). The findings indicate that longer reaction times or higher temperatures enable faster phase transformation. Therefore, temperature and time play an important role in phase transformations of the iron sulphide system. Integrating the ex situ and in situ results allowed the following reaction sequence to be established: mackinawite → greigite → smythite → pyrrhotite. Smythite occurred in the ex situ result (not appeared in the in situ result), which is because of the inhomogeneity of the solution concentrations caused by the temperature gradient via the heating apparatus in ex situ experiments. The smythite phase cannot appear when the solution concentration is uniform (like our in situ experiment). It is observed that the mackinawite phase is present at the beginning in the in situ experiment process, which is because the powerful synchrotron source is used for the in situ experiments. In this case, we can confirm the mackinawite is the first phase to appear in the formation pathways of iron sulphides and this phenomenon cannot be observed from the ex situ experiments. Compared with the ex situ experiments, the in situ experiments can be performed under an anaerobic environment. This kind of in situ XRD experiment can avoid sample oxidation because the sample was sealed in the

quartz capillary, and it can provide a high X-ray energy to obtain the strong intensity of diffraction peaks; therefore, these data from in situ XRD experiments can clarify the crystal growth of iron sulphide minerals. This can provide evidence for biogeochemical researchers and a clue for tectonic judgment.

Conclusions

In this study, we synthesized iron sulphide minerals under hydrothermal conditions at different reaction temperatures and heating times, and investigated their phase transformations and magnetic properties. Ex situ and in situ XRD results both suggested that the transformation sequence followed the order: mackinawite → greigite → smythite → pyrrhotite. Pure greigite and pyrrhotite were obtained after 1 h at 120 and 160 °C, respectively. Greigite morphology comprised irregular to granular aggregates with a particle size of ~30 nm, and pyrrhotite morphology was of stacked hexagonal sheets thousands of nanometers in width. Greigite was shown to be ferrimagnetic and pyrrhotite was anti-ferromagnetic. Based on Day's plot and MFM data, the magnetic domain of greigite was interpreted as magnetic single domain. In terms of wider implications, the greigite synthesized in this study had a competitive saturation magnetization (compared with the previous literature) and, thus, it may be useful for potential applications in biomedicine and cancer hyperthermia work.

Acknowledgements The authors would like to thank Prof. Jiin-Shuh Jean and Wei-The Jiang of the Department of Earth Sciences in the National Cheng Kung University for the help with the glove box and XRD measurements, respectively. This research received funding from the Headquarters of University Advancement at the National Cheng Kung University, which is sponsored by the Ministry of Education, Taiwan.

References

- Apostolova RD, Kolomoets OV, Shembel EM (2009) Electrolytic iron sulfides for thin-layer lithium-ion batteries. *Russ J Appl Chem* 82:1939–1943
- Beal JHL, Etchegoin PG, Tilley RD (2012) Synthesis and characterization of magnetic iron sulfide nanocrystals. *J Solid State Chem* 189:57–62
- Bourdoiseau JA, Jeannin M, Rémazeilles C, Sabot R, Refait P (2011) The transformation of mackinawite into greigite studied by raman spectroscopy. *J Raman Spectrosc* 42:496–504
- Butler EA, Peters DG, Swift EH (1958) Hydrolysis reactions of thioacetamide in aqueous solutions. *Anal Chem* 30:1379–1383
- Cahill CL, Benning LG, Barnes HL, Parise JB (2000) In situ time-resolved X-ray diffraction of iron sulfides during hydrothermal pyrite growth. *Chem Geol* 167:53–63
- Chang L, Roberts AP, Tang Y, Rainford BD, Muxworthy AR, Chen Q (2008) Fundamental magnetic parameters from pure synthetic greigite (Fe₃S₄). *J Geophys Res* 113:B06104-1–B06104-16
- Chang YS, Savitha S, Sadhasivam S, Hsu CK, Lin FH (2011) Fabrication, characterization, and application of greigite nanoparticles for cancer hyperthermia. *J Colloids Interf Sci* 363:314–319
- Chen X, Zhang X, Wan J, Wang Z, Qian Y (2005) Selective fabrication of metastable greigite (Fe₃S₄) nanocrystallites and its magnetic properties through a simple solution-based route. *Chem Phys Lett* 403:396–399
- Csákberényi-Malasics D, Rodriguez-Blanco JD, Kovács-Kis V, Rečnik A, Benning LG, Pósfai M (2012) Structural properties and transformations of precipitated FeS. *Chem Geol* 294(295):249–258
- Day R, Fuller M, Schmidt VA (1977) Hysteresis properties of titanomagnetites: grain-size and compositional dependence. *Phys Earth Planet Interior* 13:260–267
- Dekkers MJ (1988) Magnetic properties of natural pyrrhotite Part I: behaviour of initial susceptibility and saturation-magnetization-related rock-magnetic parameters in a grain-size dependent framework. *Phys Earth Planet Interior* 52:376–393
- Dekkers MJ (1989) Magnetic properties of natural pyrrhotite Part I: high- and low-temperature behavior of J_{rs} and TRM as function of grain size. *Phys Earth Planet Interior* 57:266–283
- Dekkers MJ, Schoonen MAA (1994) An electrokinetic study of synthetic greigite and pyrrhotite. *Geochim Cosmochim Acta* 58:4147–4153
- Dekkers MJ, Schoonen MAA (1996) Magnetic properties of hydrothermally synthesized greigite (Fe₃S₄)-rock magnetic parameters at room temperature. *Geophys J Int* 126:360–368
- Devey AJ (2009) Computer modelling studies of mackinawite, greigite and cubic FeS. PhD Thesis, University College London
- Dunlop DJ (2002) Theory and application of the Day plot (M_{rs}/M_s versus H_{cr}/H_c) 1. Theoretical curves and tests using titanomagnetite data. *J Geophys Res*. doi:10.1029/2001JB000486
- Erd RC, Evans HT, Richter DH (1957) Smythite, a new iron sulfide and associated pyrrhotite from Indiana. *Am Miner* 42:309–333
- Evans HT, Berner RA, Milton C (1962) Valleriite and mackinawite. *Geol Soc Am (Annual Meeting)*: 47A
- Evans HT, Milton C, Chao ECT, Adler I, Mead C, Ingram B, Berner RA (1964) Valleriite and the new iron sulfide, mackinawite. *US Geol Survey Prof Pap* 475D:64–69
- Feng M, Lu Y, Yang Y, Zhang M, Xu YJ, Gao HL, Dong L, Xu WP, Yu SH (2013) Bioinspired greigite magnetic nanocrystals: chemical synthesis and biomedicine applications. *Sci Rep* 3:2994–2999
- Fleet ME (1982) Synthetic smythite and monoclinic Fe₃S₄. *Phys Chem Miner* 8:241–246
- Frankel RB, Bazylinski DA (2003) Biologically induced mineralization by bacteria. *Rev Miner Geochem* 54:95–114
- Fu C, Bloemendal J, Qiang X, Hill MJ, An Z (2015) Occurrence of greigite in the Pliocene sediments of Lake Qinghai, China, and its paleoenvironmental and paleomagnetic implications. *Geochim Geophys Geosyst* 16:1296–1306
- Gao S, Huang F, Song D, Li G, Liu Q, Feng T, Zhao R, Liu J, Gao W (2015) Growth mechanism and stability study on the Fe₃S₄ nanocrystals synthesized under thermal and humid conditions. In: *Proceedings of the 11th international congress for applied mineralogy*, pp 115–123
- Gong MG, Kirkeminde A, Xie Y, Lu R, Liu J, Wu JZ, Ren S (2013) Iron pyrite (FeS₂) broad spectral and magnetically responsive photodetectors. *Adv Opt Mater* 1:78–83
- Gupta PR (1965) Pyrrhotite geothermometry and its application to the sulfide ores of the Mosabani Mines, Singhbhum, Bihar, India. *Econ Geol* 60:175–180

- Harrison RM (2008) Understanding our environment: an introduction to environmental chemistry and pollution. Cambridge University Press, UK
- He ZB, Yu SH, Zhou XY, Li XG, Qu JF (2006) Magnetic-field-induced phase-selective synthesis of ferrosulfide microrods by a hydrothermal process: microstructure control and magnetic properties. *Adv Funct Mater* 16:1105–1111
- Hoffmann V (1992) Greigite (Fe_3S_4): magnetic properties and first domain observations. *Phys Earth Planet Interior* 70:288–301
- Holmes J (1999) Fate of incorporated metals during mackinawite oxidation in sea water. *Appl Geochem* 14:277–281
- Jeong HY, Lee JH, Hayes KF (2008) Characterization of synthetic nanocrystalline mackinawite: crystal structure, particle size, and specific surface area. *Geochim Cosmochim Acta* 72:493–505
- Johannsen M, Gneveckow U, Eckelt L, Feussner A, Waldöfner N, Scholz R, Deger S, Wust W, Loening SA, Jordan A (2005) Clinical hyperthermia of prostate cancer using magnetic nanoparticles: presentation of a new interstitial technique. *Int J Hypertherm* 21:637–647
- Kontny A, Wall HD, Sharp TG, Posfai M (2000) Mineralogy and magnetic behavior of pyrrhotite from a 260 C section at the KTB drilling site, Germany. *Am Miner* 85:1416–1427
- Krupp RE (1994) Phase relations and phase transformations between the low-temperature iron sulfides mackinawite, greigite, and smythite. *Eur J Miner* 6:265–278
- Lennie AR, Redfern SAT, Schofield PF, Vaughan DJ (1995) Synthesis and Rietveld crystal structure refinement of mackinawite, tetragonal FeS . *Miner Mag* 59:677–683
- Lennie AR, Redfern SAT, Champness PE, Stoddart CP, Schofield PF, Vaughan DJ (1997) Transformation of mackinawite to greigite: an in situ X-ray powder diffraction and transmission electron microscope study. *Am Miner* 82:302–309
- Letard I, Sainctavit P, Menguy N, Valet JP, Isambert A, Dekkers M, Gloter A (2005) Mineralogy of greigite Fe_3S_4 . *Phys Scr T* 115:489–491
- Li F (1996) Studies of structures and phase transitions in pyrrhotite. Thesis of Iowa State University
- Li T, Li H, Wu Z, Hao H, Liu J, Huang T, Sun H, Zhang J, Zhang H, Guo Z (2015) Colloidal synthesis of greigite nanoplates with controlled lateral size for electrochemical applications. *Nanoscale* 7:4171–4178
- Morimoto N, Gyobu A, Mukaiyama H, Izawa E (1975) Crystallography and stability of pyrrhotites. *Econ Geol* 70:824–833
- Mullet M, Boursiquot S, Ehrhardt JJ (2004) Removal of hexavalent chromium from solutions by mackinawite, tetragonal FeS . *Colloids Surf A* 244:77–85
- Muxworthy AR, Williams W (2009) Critical superparamagnetic/single-domain grain sizes in interacting magnetite particles: implications for magnetosome crystals. *J R Soc Interf* 6:1207–1212
- Muxworthy AR, Williams W, Roberts AP, Winklhofer M, Chang L, Posfai M (2013) Critical single domain grain sizes in chains of interacting greigite particles: implications for magnetosome crystals. *Geochim Geophys Geosyst* 14:5430–5441
- Nekrasov IJ, Besmen NI (1979) Pyrite-pyrrhotite geothermometer. Distribution of cobalt, nickel and tin. *Phys Chem Earth* 11:767–771
- O'Reilly W, Hoffmann V, Chouker AC, Soffel HC, Menyeh A (2000) Magnetic properties of synthetic analogues of pyrrhotite ore in the grain size range 1–24 μm . *Geophys J Int* 142:669–683
- Paoletta A, George C, Povia M, Zhang Y, Krahne R, Gich M, Genovesi A, Falqui A, Longobardi M, Guardia P, Pellegrino T, Manna L (2011) Charge transport and electrochemical properties of colloidal greigite (Fe_3S_4) nanoplatelets. *Chem Mater* 23:3762–3768
- Parry LG (1982) Magnetization of immobilized particle dispersions with two distinct particle sizes. *Phys Earth Planet Interior* 28:230–241
- Rickard DT (1968) Synthesis of smythite—rhombohedral Fe_3S_4 . *Nature* 218:356–357
- Rickard D, Luther GW (2007) Chemistry of iron sulfides. *Chem Rev* 107:514–562
- Roberts AP, Weaver R (2005) Multiple mechanisms of remagnetization involving sedimentary greigite (Fe_3S_4). *Earth Planet Sci Lett* 231:263–277
- Roberts AP, Chang L, Rowan CJ, Horng CS, Florindo F (2011) Magnetic properties of sedimentary greigite (Fe_3S_4): an update. *Rev Geophys* 49:1–46
- Rowan CJ, Roberts AP, Broadbent T (2009) Reductive diagenesis, magnetite dissolution, greigite growth and paleomagnetic smoothing in marine sediments: a new view. *Earth Planet Sci Lett* 277:223–235
- Schoonen MAA, Barnes HL (1991) Mechanisms of pyrite and marcasite formation from solution: III: hydrothermal processes. *Geochim Cosmochim Acta* 55:3491–3504
- Schwarz EJ, Vaughan DJ (1972) Magnetic phase relations of pyrrhotite. *J Geomag Geoelectr* 24:441–458
- Sharma SK (2012) Green corrosion chemistry and engineering: opportunities and challenges. Wiley, Weinheim
- Sines IT, Vaughn DD II, Misra R, Popczun EJ, Schaak RE (2012) Synthesis of tetragonal mackinawite-type FeS nanosheets by solvothermal crystallization. *J Solid State Chem* 196:17–20
- Skinner BJ, Erd RC, Grimaldi FS (1964) Greigite, the thio-spinel of iron; a new mineral. *Am Miner* 49:543–555
- Spender MR, Coey JMD, Morrish AH (1972) The magnetic properties and Mössbauer spectra of synthetic samples of Fe_3S_4 . *Can J Phys* 50:2313–2326
- Taylor LA (1970) Smythite, $\text{Fe}_{3+x}\text{S}_4$, and associated minerals from the Silverfields mine, Cobalt, Ontario. *Am Miner* 55:1650–1658
- Taylor LA, Williams KL (1972) Smythite (Fe, Ni) $_9\text{S}_{11}$ —a redefinition. *Am Mineral* 57:1571–1577
- Taylor P, Rummery TE, Owen DG (1979) On the conversion of mackinawite to greigite. *J Inorg Nucl Chem* 41:595–596
- Uda M (1965) On the synthesis of greigite. *Am Miner* 50:1487–1489
- Vallejo-Fernandez G, Whear O, Roca AG, Hussain S, Timmis J, Patel V, O'Grady K (2013) Mechanisms of hyperthermia in magnetic nanoparticles. *J Phys D Appl Phys* 46:312001–312006
- Watson JHP, Ellwood DC, Deng Q, Mikhailovsky S, Hayter CE, Evans J (1995) Heavy metal adsorption on bacterially produced FeS . *Miner Eng* 8:1097–1108
- White LM, Bhartia R, Stucky GD, Kanik I, Russell MJ (2015) Mackinawite and greigite in ancient alkaline hydrothermal chimneys: identifying potential key catalysts for emergent life. *Earth Planet Sci Lett* 430:105–114
- Wolthers M, Charlet L, van Der Weijden CH, van der Linde PR, Rickard D (2005) Arsenic mobility in the ambient sulfidic environment: sorption of arsenic(V) and arsenic(III) onto disordered mackinawite. *Geochim Cosmochim Acta* 69:3483–3492
- Yuan B, Fu H, Luan W (2012) One-step synthesis of Fe_3S_4 microcrystals and its facile transformation to Fe_7S_8 microcrystals. *Appl Mech Mater* 130–134:1270–1275
- Zhang ZJ, Chen XY (2009) Magnetic greigite (Fe_3S_4) nanomaterials: shape-controlled solvothermal synthesis and their calcination conversion into hematite ($\alpha\text{-Fe}_2\text{O}_3$) nanomaterials. *J Alloys Compd* 488:339–345